

DNA Binding and Anti-Cancer Activity of Redox-Active Heteroleptic Piano-Stool Ru(II), Rh(III), and Ir(III) Complexes Containing 4-(2-Methoxypyridyl)phenyldipyrrromethene

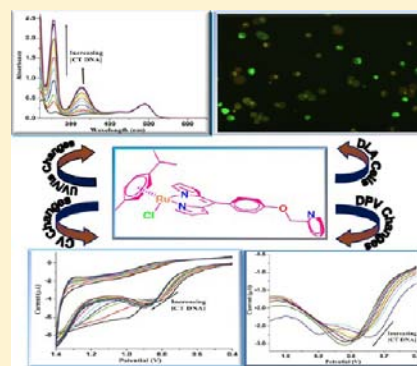
Rakesh Kumar Gupta,[†] Rampal Pandey,[†] Gunjan Sharma,[§] Ritika Prasad,[§] Biplob Koch,[§] Saripella Srikrishna,[‡] Pei-Zhou Li,[‡] Qiang Xu,[‡] and Daya Shankar Pandey^{*†}

[†]Department of Chemistry, [‡]Department of Biochemistry, and [§]Department of Zoology, Faculty of Science, Banaras Hindu University, Varanasi, 221 005 Uttar Pradesh, India

[‡]National Institute of Advanced Industrial Science and Technology (AIST), 1-8-31, Midorigaoka, Ikeda, Osaka 563-8577, Japan

Supporting Information

ABSTRACT: The synthesis of four novel heteroleptic dipyrinato complexes $[(\eta^6\text{-arene})\text{RuCl}(2\text{-pcdpm})]$ ($\eta^6\text{-arene} = \text{C}_6\text{H}_6$, **1**; $\text{C}_{10}\text{H}_{14}$, **2**) and $[(\eta^5\text{-C}_5\text{Me}_5)\text{MCl}(2\text{-pcdpm})]$ ($\text{M} = \text{Rh}$, **3**; Ir , **4**) containing a new chelating ligand 4-(2-methoxypyridyl)phenyldipyrrromethene (2-pcdpm) have been described. The complexes **1–4** have been fully characterized by various physicochemical techniques, namely, elemental analyses, spectral (ESI-MS, IR, ^1H , ^{13}C NMR, UV/vis) and electrochemical studies (cyclic voltammetry (CV) and differential pulse voltammetry (DPV)). Structures of **3** and **4** have been determined crystallographically. In vitro antiproliferative and cytotoxic activity of these complexes has been evaluated by trypan blue exclusion assay, cell morphology, apoptosis, acridine orange/ethidium bromide (AO/EtBr) fluorescence staining, and DNA fragmentation assay in Dalton lymphoma (DL) cell lines. Interaction of **1–4** with calf thymus DNA (CT DNA) has also been supported by absorption titration and electrochemical studies. Our results suggest that in vitro antitumor activity of **1–4** lies in the order $2 > 1 > 4 > 3$.



INTRODUCTION

Metal based compound cisplatin is one of the most widely used drugs for treatment of cancer.¹ Despite wide applicability this wonderful drug is associated with high toxicity leading to severe side effects and acquired drug resistance.² To overcome these problems attempts are being made to develop alternatives for platinum based drugs having better prospects, such as oral administration, and lower side effects and clinical costs.³ In this context, complexes based on several transition and non-transition metals have been investigated. Among these, ruthenium has shown great promise because of its variable oxidation states, low toxicity, selectivity for cancer cells, and ability to mimic iron in binding to biomolecules.⁴ It has been observed that a number of ruthenium complexes show high in vivo and/or in vitro antitumor activity among which KP1019 and NAMI-A present most fascinating next-generation anticancer drugs in clinical trials.⁵ Notably, these exhibit exciting antitumor properties, and the treatment is not accompanied by major drug related side effects.^{2–4} Further, it has been shown that organometallic half-sandwich Ru(II), Rh(III), and Ir(III) complexes exhibit excellent in vitro and in vivo anticancer property, but still need to be explored further.⁶ Sadler et al. have clearly shown that cationic arene ruthenium(II) complexes of the type $[(\eta^6\text{-arene})\text{Ru}(\text{en})(\text{Cl})]^+$ ($\text{en} = \text{ethylenediamine}$) exhibit excellent anticancer activity.⁷ Further, they demonstrated that replacement of chelating ethylenedi-

amine by 2,2'-bipyridine (bipy) and its derivatives make the ensuing complexes almost inactive toward human ovarian and lung cancer cell lines.⁸ However, replacement of ethylenediamine by acetylacetonone or a bipyridine diol leads to noticeable enhancement in cytotoxicity.⁹ In addition, size of the arene ligand also influences anticancer activity to a large extent.¹⁰ As the arene and ancillary ligands play a crucial role in determining anticancer activity of ruthenium complexes, attempts are being made to fine-tune their pharmacological properties by systematic variation of these building blocks.¹¹

Further, dipyrromethenes (dipyrin) are highly conjugated planar aromatic bidentate N,N -donor ligands analogous to ethylenediamine, 2,2'-bipyridine, or 1,10-phenanthroline¹² and are widely used in the synthesis of numerous stable, neutral homo- and heteroleptic complexes with a variety of metal ions.¹³ The half-sandwich ruthenium, rhodium, and iridium complexes containing η^6 -bonded arene and N,N -chelating ligands find wide applications in bio-organometallic chemistry.¹⁴ Although a large number of arene ruthenium and structurally related rhodium and iridium dipyrinato complexes have been reported, their anticancer properties have not been explored so far.¹⁵

Received: October 9, 2012

Published: March 11, 2013

Furthermore, spontaneous animal tumors mimic human malignancy closely; therefore, they serve as ideal tumor models for various investigative purposes. Dalton's lymphoma (DL) is a T cell tumor that originates in thymus gland of *Dolichos biflorus* agglutinin (DBA) strain (H-2^d) of mouse.¹⁶ It is transplantable and characterized by a highly invasive nature.¹⁷ With the objective of developing anticancer agents, we have synthesized four new complexes $[(\eta^6\text{-arene})\text{RuCl}(\text{2-pcdpm})]$ (arene = C₆H₆, **1**; C₁₀H₁₄, **2**), $[(\eta^5\text{-C}_5\text{Me}_5)\text{MCl}(\text{2-pcdpm})]$ (M = Rh, **3**; Ir, **4**) containing a planar dipyrinato ligand and examined their effect on DL cancer cells. In addition, the object of preparing methoxypyridyl group over any other moiety is based on the possibility of their noncovalent interaction through pyridyl nitrogen and etheratic oxygen with DNA. Also, the planar dipyrin core may stack/intercalate with DNA. Through this contribution we report the synthesis, characterization and in vitro anticancer activity of Ru(II), Rh(III), and Ir(III) complexes **1–4** on DL cells.

EXPERIMENTAL SECTION

Reagents. All the synthetic manipulations were performed under nitrogen atmosphere. Solvents were dried and distilled prior to their use following standard procedures.¹⁸ Hydrated RuCl₃·xH₂O, RhCl₃·xH₂O, IrCl₃·xH₂O, 1,3-hexadiene, α -phellandrene, pentamethylcyclopentadiene, 2,3-dichloro-5,6-dicyano-1,4-benzoquinone (DDQ), 4-hydroxybenzaldehyde, 2-picolychloride, and pyrrole were procured from Sigma Aldrich Chemical Co. Pvt. Ltd., and used as received without further purifications. Ethylenediaminetetraacetic acid (EDTA) and ethidium bromide (EtBr) were obtained from Loba Chemie, acridine orange (AO) from Sisco Research Laboratory (SRL), and agarose from Hi-Media Laboratories, Mumbai, India. Calf thymus (CT) DNA was purchased from Bangalore Genei, India. The precursor complexes $[(\eta^6\text{-arene})\text{Ru}(\mu\text{-Cl})\text{Cl}]_2$ ($\eta^6\text{-arene}$ = C₆H₆, C₁₀H₁₄), $[(\eta^5\text{-C}_5\text{Me}_5)\text{M}(\mu\text{-Cl})\text{Cl}]_2$ (M = Rh or Ir) and 4-(pyridin-2-ylmethoxy)-benzaldehyde were prepared and purified following the literature procedures.¹⁹

General Methods. Elemental analyses for carbon, hydrogen, and nitrogen were performed on an Exeter Analytical Inc. model CE-440 CHN analyzer. Infrared and electronic absorption spectra were acquired on a Varian 3300 FT-IR and Shimadzu UV-1601, respectively. ¹H (300 MHz), ¹³C (75.45 MHz), and ¹H-¹H COSY (300 MHz) NMR spectra at room temperature (rt) were obtained on a JEOL AL300 FT-NMR spectrometer using tetramethylsilane [Si(CH₃)₄] as an internal reference. Electrospray ionization mass spectrometric (ESI-MS) measurements were made on a THERMO Finnigan LCQ Advantage Max ion trap mass spectrometer. Samples (10 μ L) were dissolved in dichloromethane/acetonitrile (3:7, v/v) and introduced into the ESI source through a Finnigan surveyor auto sampler. Mobile phase (MeOH/MeCN: H₂O, 90:10) flowed at a rate of 250 μ L/min. The ion spray voltage was set at 5.3 KV and capillary voltage at 34 V. The MS scan run up to 2.5 min and spectra print outs were averaged of over 10 scans. Electrochemical measurements were performed on a CHI 620c electrochemical analyzer as described earlier.²⁰

Synthesis of 4-(2-Methoxypyridyl)phenyldipyrromethane. A degassed solution of 4-(2-methoxypyridyl)benzaldehyde (2.13 g, 10.0 mmol) in pyrrole (6.9 mL, 100.0 mmol) was treated with catalytic amounts of trifluoroacetic acid (15.4 μ L, 0.20 mmol) and stirred for 1 h under nitrogen atmosphere and then heated at 70 °C overnight. The reaction mixture was diluted with CH₂Cl₂ (50 mL) washed with 0.1 M NaOH (50 mL) followed by water (50 mL) and dried over Na₂SO₄. After removal of the solvent under reduced pressure, residual pyrrole was removed by vacuum distillation with gentle heating. The ensuing product upon purification by column chromatography (SiO₂; hexanes: CH₂Cl₂, 1:1) gave the desired compound as a white solid. Yield: 72% (2.34 g). Anal. Calc for C₂₁H₁₇N₃O requires: C, 77.28; H, 4.94; N, 12.87. Found: C, 77.15; H, 4.89; N, 12.85%. ¹H NMR (CDCl₃, δ

ppm): 5.18 (s, 2H, OCH₂), 5.42 (s, 1H, CH, *meso*), 5.90 (s, 2H, pyrrolic), 6.14 (m, 2H, pyrrolic), 6.68 (s, 2H, pyrrolic), 6.92 (m, 2H, phenyl), 7.11 (m, 2H, phenyl), 7.22 (m, 1H, pyridyl), 7.52 (d, 1H, J = 7.8 Hz, pyridyl), 7.72 (t, 1H, pyridyl), 7.95 (bs, 2H, NH, pyrrolic), 8.58 (d, 1H, J = 7.2 Hz, pyridyl). ¹³C NMR (CDCl₃, δ ppm): 42.9 (C-5), 69.7 (C-10), 106.8 (2a), 106.9 (2b), 108.0 (3a), 108.1 (3b), 114.7 (1a), 115.4 (1b), 117.1 (7a), 117.2 (7b), 121.7 (C-6), 123.0 (C-14), 129.3 (4a), 132.9 (C-4b), 133.7 (8a), 134.9 (C-8b), 137.6 (C-12), 148.3 (C-13), 154.9 (C-11), 156.8 (C-15), 163.1 (C-9). IR (KBr pellets, cm⁻¹; % T): 588 (59), 676 (52), 733 (28), 744 (32), 825 (55), 998 (38), 1034 (37, $\nu\text{C-O}_{\text{aliphatic}}$), 1145 (52), 1212 (28, $\nu\text{C-O}_{\text{aromatic}}$), 1339 (48, $\nu\text{C=C}$), 1375 (42, $\nu\text{C=C}$), 1545 (35, $\nu\text{C=N}_{\text{pyrrolic}}$), 1608 (28, $\nu\text{C=N}_{\text{pyridyl}}$), 1650 (46).

Synthesis of $[(\eta^6\text{-C}_6\text{H}_6)\text{RuCl}(\text{2-pcdpm})]$ (1**).** To an ice cold solution of 4-(2-methoxypyridyl)phenyldipyrromethane (0.328 g, 1.0 mmol) in CH₂Cl₂ (60 mL), DDQ (0.227 g, 1.0 mmol) dissolved in benzene (30 mL) was added slowly with stirring over a period of 1 h. After completion of the reaction (confirmed by TLC), solvent was removed under reduced pressure, and the dark red residue thus obtained redissolved in CH₂Cl₂/MeOH (70 mL; 1:1 v/v). Triethylamine (1.0 mL) and dimeric complex $[(\eta^6\text{-C}_6\text{H}_6)\text{Ru}(\mu\text{-Cl})\text{Cl}]_2$ (0.250 g, 0.50 mmol) were added successively to this solution, and reaction mixture was stirred at rt for ~4 h. After filtration, the solvent was removed under reduced pressure, and the resulting residue purified by flash column chromatography (SiO₂, CH₂Cl₂ with 2% MeOH) to afford complex **1** as a red solid. Yield: 48% (0.300 g). Anal. Calc for C₂₇H₂₂N₃OClRu, requires: C, 59.94; H, 4.10; N, 7.77. Found: C, 59.85; H, 4.33; N, 7.53%. ¹H NMR (CDCl₃, δ ppm): 5.27 (s, 2H, OCH₂), 5.37 (s, 6H, benzene), 6.43 (d, 2H, J = 2.7 Hz, pyrrolic), 6.57 (d, 2H, J = 3.3 Hz, pyrrolic), 7.03 (d, 2H, J = 7.8 Hz, pyrrolic), 7.35 (d, 2H, J = 8.4 Hz, phenyl), 7.57 (d, 2H, J = 7.8 Hz, phenyl), 7.65 (s, 2H, pyridyl), 7.74 (d, 1H, J = 4.2 Hz, pyridyl), 8.61 (s, 1H, pyridyl). ¹³C NMR (CDCl₃, δ ppm): 43.7 (C-5), 70.9 (C-10) 85.1 (benzene) 107.7 (C-2), 113.7 (C-3a), 114.7 (C-3b), 117.9 (C-1), 123.9 (C-8), 130.9 (C-7), 132.7 (C-4), 134.5 (C-6), 137.6 (C-12), 142.5 (C-13), 147.9 (C-11), 152.3 (C-15), 158.9 (C-9). ESI-MS. (Calcd, found, *m/z*) 506.0806, 506.0030 [M-Cl]⁺. IR (KBr pellets, cm⁻¹; % T): 714 (51), 728 (50), 994 (33), 1026 (28, $\nu\text{C-O}_{\text{aliphatic}}$), 1175 (53), 1206 (54), 1249 (27, $\nu\text{C-O}_{\text{aromatic}}$), 1344 (29, $\nu\text{C=C}_{\text{pyrrolic}}$), 1378 (28, $\nu\text{C=C}_{\text{pyridyl}}$), 1409 (48), 1505 (49), 1547 (27, $\nu\text{C=N}_{\text{pyrrolic}}$), 1605 (29, $\nu\text{C=N}_{\text{pyridyl}}$), 2924 (53), 2961 (54). UV/vis. (*c*, 10 μ M; EtOH:H₂O, 1:1, v: v; pH ~7.3; λ_{max} nm, ϵ M⁻¹ cm⁻¹): 487 (2.94 \times 10⁴), 432 (1.19 \times 10⁴), 358 (0.85 \times 10⁴), 260 (1.11 \times 10⁴).

Synthesis of $[(\eta^6\text{-C}_{10}\text{H}_{14})\text{RuCl}(\text{2-pcdpm})]$ (2**).** It was prepared following the above procedure for **1** except that $[(\eta^6\text{-C}_{10}\text{H}_{14})\text{Ru}(\mu\text{-Cl})\text{Cl}]_2$ (0.306 g, 0.50 mmol) was used in place of $[(\eta^6\text{-C}_6\text{H}_6)\text{Ru}(\mu\text{-Cl})\text{Cl}]_2$ (0.250 g, 0.50 mmol). Yield: 52% (0.310 g). Anal. Calc for C₃₁H₃₀ClN₃ORu, requires: C, 62.36; H, 5.06; N, 7.04. Found: C, 62.21; H, 5.12; N, 6.91%. ¹H NMR (CDCl₃, δ ppm): 1.11 (d, 6H, J = 7.9 Hz, *p*-cymene CH(CH₃)₂), 2.26 (s, 3H, *p*-cymene CH₃), 2.40 (m, 1H, *p*-cymene CH(CH₃)₂), 5.30 (s, 2H, -OCH₂), 5.34 (s, 4H, *p*-cymene C₆H₄), 6.50 (d, 2H, J = 3.6 Hz, pyrrolic), 6.67 (d, 2H, J = 3.6 Hz, pyrrolic), 7.05 (d, 2H, J = 8.4 Hz, pyrrolic), 7.37 (d, 2H, J = 8.4 Hz, phenyl), 7.61 (d, 2H, J = 7.8 Hz, phenyl), 7.79 (m, 1H, pyridyl), 8.03 (s, 3H), 8.66 (d, 1H, J = 3.9 Hz). ¹³C NMR (CDCl₃, δ ppm): 18.6 (*p*-cymene CH(CH₃)₂), 22.1 (*p*-cymene CH₃), 30.5 (*p*-cymene CH(CH₃)₂), 44.9 (C-5) 70.6 (C-10), 84.6, 84.8, 100.3, 101.9 (*p*-cymene C₆H₄), 107.5 (C-2), 113.6 (C-3), 118.2 (C-1), 121.4 (C-8), 130.9 (C-4, C-6), 131.7 (C-12), 135.3 (C-13, C-14), 154.6 (C-11, C-15), 156.9 (C-9). ESI-MS. (Calcd, found, *m/z*) 562.1432, 562.1433 [M-Cl]⁺. IR (KBr pellets, cm⁻¹; % T): 713 (50), 729 (49), 995 (32), 1027 (24, $\nu\text{C-O}_{\text{aliphatic}}$), 1174 (44), 1206 (45), 1248 (24, $\nu\text{C-O}_{\text{aromatic}}$), 1342 (28, $\nu\text{C=C}_{\text{pyrrolic}}$), 1377 (29, $\nu\text{C=C}_{\text{pyridyl}}$), 1405 (48), 1504 (47), 1546 (27, $\nu\text{C=N}_{\text{pyrrolic}}$), 1604 (23, $\nu\text{C=N}_{\text{pyridyl}}$), 2924 (58), 2960 (60). UV/vis. (*c*, 10 μ M; EtOH:H₂O, 1:1, v: v; pH ~7.3; λ_{max} nm, ϵ M⁻¹ cm⁻¹): 489 (3.47 \times 10⁴), 431 (1.44 \times 10⁴), 351 (1.18 \times 10⁴), 260 (1.73 \times 10⁴).

Synthesis of $[(\eta^5\text{-C}_5\text{Me}_5)\text{RhCl}(\text{2-pcdpm})]$ (3**).** It was prepared following the above procedure for **1** except that $[(\eta^5\text{-C}_5\text{Me}_5)\text{Rh}(\mu\text{-Cl})\text{Cl}]_2$ (0.309 g, 0.50 mmol) was used in place of $[(\eta^6\text{-C}_6\text{H}_6)\text{Ru}(\mu\text{-Cl})\text{Cl}]_2$ (0.306 g, 0.50 mmol).

Cl)Cl₂] (0.250 g, 0.50 mmol). Yield: 54% (0.323 g). Microanalytical data: C₃₁H₃₁N₃OClRh, requires: C, 45.88; H, 4.66; N, 8.45. Found: C, 45.45; H, 4.53; N, 8.33%. ¹H NMR (CDCl₃, δ ppm): 1.48 (s, 15H, Cp* CH₃), 5.28 (s, 2H, OCH₂), 6.48 (d, 2H, J = 1.2 Hz, pyrrolic), 6.72 (d, 2H, J = 4.2 Hz, pyrrolic), 7.03 (d, 2H, J = 8.4 Hz, pyrrolic), 7.28 (1H, pyridyl, merged with CDCl₃), 7.36 (d, 2H, J = 8.4 Hz, phenyl), 7.57 (d, 1H, J = 7.8 Hz, pyridyl), 7.73 (s, 1H, pyridyl), 7.77 (s, 2H, phenyl), 8.62 (d, 1H, J = 4.5 Hz, pyridyl). ¹³C NMR (CDCl₃, δ ppm): 8.5 (Cp* CH₃), 45.2 (C-5), 48.5 (C-10), 94.4 (Cp* Rh-C), 94.5 (Cp* Rh-C), 107.2 (C-2), 113.6 (C-3a), 114.3 (C-3b), 118.7 (C-1), 129.3 (C-8), 131.7 (C-7), 132.7 (C-4), 136.1 (C-6), 137.6 (C-12), 147.0 (C-14), 148.0 (C-13), 151.3 (C-11), 152.5 (C-15), 159.3 (C-9). ESI-MS (Calcd, found, m/z): 564.1522, 564.1526 [M-Cl]⁺. IR (KBr pellets, cm⁻¹; % T): 713 (30), 727 (31), 769 (31), 809 (23), 886 (45), 934 (51), 989 (13), 1018 (8, νC–O_{aliphatic}), 1175 (33), 1250 (8, νC–O_{aromatic}), 1282 (49), 1338 (11, νC=C_{pyrrolic}), 1372 (15, νC=C_{pyridyl}), 1400 (32), 1448 (41), 1503 (32), 1541 (9, νC=N_{pyrrolic}), 1574 (34), 1606 (25, νC=N_{pyridyl}), 2916 (48). UV/vis. (c, 10 μM; EtOH:H₂O, 1:1, v/v; pH ~7.3; λ_{max} nm, ε M⁻¹ cm⁻¹): 488 (3.56 × 10⁴), 436 (1.97 × 10⁴), 353 (1.85 × 10⁴), 259 (1.76 × 10⁴).

Synthesis of [(η⁵-C₅Me₅)IrCl(2-pcdpm)] (4). Complex 4 was prepared following the above procedure for 1 except that [(η⁵-C₅Me₅)Ir(μ-Cl)Cl₂] (0.309 g, 0.50 mmol) was used in place of [(η⁶-C₆H₆)Ru(μ-Cl)Cl₂] (0.250 g, 0.50 mmol). Yield: 55% (0.378 g). Microanalytical data: C₃₁H₃₁ClN₃OIr, requires: C, 54.12; H, 4.53; N, 6.10. Found: C, 54.24; H, 4.76; N, 6.23%. ¹H NMR (CDCl₃, δ ppm): 1.48 (s, 15H, Cp* CH₃), 5.28 (s, 2H, OCH₂), 6.44 (d, 2H, J = 1.2 Hz, pyrrolic), 6.57 (d, 2H, J = 3.3 Hz, pyrrolic), 7.04 (d, 2H, J = 5.4 Hz, pyrrolic), 7.26 (1H, pyridyl, merged with CDCl₃), 7.36 (d, 2H, J = 8.4 Hz, phenyl), 7.58 (d, 1H, J = 7.8 Hz, pyridyl), 7.65 (s, 2H, phenyl), 7.76 (t, 1H, pyridyl), 8.62 (d, 1H, J = 4.5 Hz, pyridyl). ¹³C NMR (CDCl₃, δ ppm): 8.6 (Cp* CH₃), 45.9 (C-5), 48.1 (C-10), 94.5 (Cp* Ir-C), 94.6 (Cp* Ir-C), 109.7 (C-2), 113.6 (C-3), 118.9 (C-1), 121.4 (C-8), 122.8 (C-7), 131.0 (C-4), 131.8 (C-6), 132.7 (C-12), 136.0 (C-14), 136.9 (C-13), 149.2 (C-11), 152.8 (C-15), 159.2 (C-9). ESI-MS (Calcd, found, m/z): 654.2096, 654.2090 [M-Cl]⁺. IR (KBr pellets, cm⁻¹): IR (KBr pellets, cm⁻¹; % T): 713 (53), 729 (54), 769 (51), 817 (50), 888 (37), 935 (59), 993 (37), 1022 (32, νC–O_{aliphatic}), 1174 (51), 1251 (32, νC–O_{aromatic}), 1284 (53), 1341 (37, νC=C_{pyrrolic}), 1375 (37, νC=C_{pyridyl}), 1403 (48), 1450 (51), 1504 (48), 1542 (35, νC=N_{pyrrolic}), 1574 (48), 1605 (31, νC=N_{pyridyl}), 2918 (54). UV/vis. (c, 10 μM; EtOH:H₂O, 1:1, v/v; pH ~7.3; λ_{max} nm, ε M⁻¹ cm⁻¹): 496 (3.33 × 10⁴), 413 (1.30 × 10⁴), 357 (1.66 × 10⁴), 260 (2.27 × 10⁴).

X-ray Structure Determination. Crystals suitable for single crystal X-ray diffraction analyses for 3 and 4 were obtained by slow diffusion of hexane over dichloromethane solution of the respective complexes. X-ray data were collected on a R-AXIS RAPID II diffractometer (153 K) with Mo-Kα radiation (λ = 0.71073 Å) at the single crystal X-diffraction center of the National Institute of Advanced Industrial Science and Technology (AIST), Osaka, Japan. Structures were solved by direct methods (SHELXS 97) and refined by full-matrix least-squares on F² (SHELX 97).²¹ All the non-H atoms were treated anisotropically. H-atoms attached to carbon were included as a fixed contribution and were geometrically calculated and refined using the SHELX riding model. The computer program PLATON was used for analyzing the interaction and stacking distances.²² CCDC deposition Nos. 879367 (3) and 879368 (4) contain supplementary crystallographic data for this paper. The data can be obtained free of charge from <http://www.ccdc.cam.ac.uk/conts/retrieving.html> or from the CCDC, 12 Union Road, Cambridge CB2 1EZ, U.K.; Fax: + 44-1223-336033; E-mail: deposit@ccdc.cam.ac.uk.

UV/vis Studies. UV/visible absorption titration studies have been performed using a fixed concentration of the complexes (10 μM, EtOH/H₂O, 1:1, v/v) and varying the CT DNA concentration (Na-phosphate buffer solution, pH ~7.2). The purity of DNA has been established by following the absorption ratio of the bands at 260 and 280 nm. It was found to be 1.9:1, suggesting that CT DNA is sufficiently free from protein. Further, the concentration of CT DNA was determined by UV/vis absorbance and molar absorption

coefficient (6600 M⁻¹ cm⁻¹) at ~260 nm. The strength of interaction between complexes and CT DNA was monitored by the change in the absorption intensity of the band associated with π–π* (~260 nm) transitions. The equilibrium binding constant (K_b) and the binding site size (s, per base pair) have been determined by nonlinear least-squares analysis of the isotherm using the equation of Bard and co-workers based on the McGhee–von Hippel (MvH) model,²³

$$(\epsilon_a - \epsilon_f)/(\epsilon_b - \epsilon_f) = (b - (b^2 - 2K_b^2 Ct[\text{DNA}]/s)^{1/2})/2K_b Ct$$

where $b = 1 + K_b Ct + K_b [\text{DNA}]/2s$, ϵ_a is the extinction coefficient observed for spectral band at a given DNA concentration, ϵ_f is the extinction coefficient of the complex in solution, ϵ_b is the extinction coefficient of the complex when fully bound to DNA, K_b is the equilibrium binding constant, Ct is the total complex concentration, [DNA] is the DNA concentration in nucleotides, and s is the binding site size of complexes in base pairs. The non linear least-squares fit analysis was performed using Origin Lab software.

Electrochemical Measurements. The electrochemical behavior of 1–4 has been followed by cyclic and differential pulse voltammetry (MeCN, 100 μM) in the potential range +1.4 to –2.0 V at a scan rate of 50 mV s⁻¹. The measurements were performed at rt using tetrabutylammonium perchlorate [(n-Bu)₄N]ClO₄ (0.1 M) as a supporting electrolyte, and redox potentials were referenced to the Fc/Fc⁺ couple (0.1 V). Electrochemical titration experiments have been performed at rt to understand the binding behavior by varying the concentration of CT DNA (Na-phosphate buffer solution, pH ~7.2) and keeping complex concentrations constant.

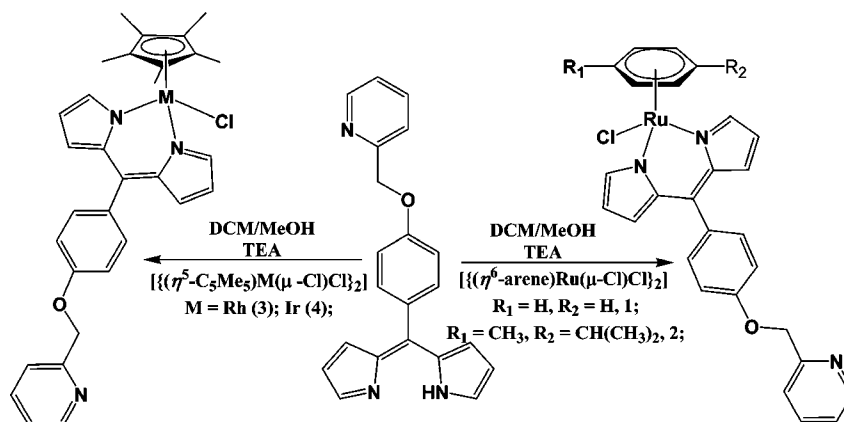
Partition Coefficient Determination. The lipophilicity of 1–4 was measured by the “shake flask” method between octanol/water phase partitions.²⁴ Octanol-saturated water (OSW) and water-saturated octanol (WSO) were prepared using analytical grade octanol (Merck) and double distilled water. Complexes 1–4 (1 mg/mL) in a mixture of ethanol and water (1:4) were diluted to 2, 4, 6, 8, 10 μg/mL in water, and alternatively 1–4 (1 mg/mL) were diluted to 2, 4, 6, 8, 10 μg/mL in octanol, respectively. Triplicate experiments have been performed for each complex, and their absorbance determined (487, 1; 489, 2; 507, 3; 309 nm 4 in octanol, and 492, 1; 493, 2; 498, 3; 305 nm 4 in water) to draw the calibration curve (Supporting Information, Figures S1–S8). Appropriate amounts of 1–4 (4 mg/mL) in equal volume (50:50) were shaken for 24 h at rt. After attaining equilibrium the organic and aqueous phases were separated and centrifuged. Finally, the concentration of the drug in each phase was determined by UV/visible spectroscopy at their respective wavelength (mentioned above). The sample solution concentration was used to calculate log P. Partition coefficients for 1–4 were calculated using the equation $\log P = \log [(1-4)_{\text{oct}} / (1-4)_{\text{aq}}]$.²⁵

Trypan Blue Exclusion Assay. For the in vitro cytotoxicity assay, 1 × 10⁶ viable Dalton’s Lymphoma Ascite (DLA) cells (maintained by serial transplantations in Swiss albino mice by intraperitoneal transplantation) were suspended in phosphate buffer saline (PBS) and incubated with increasing concentration of 1–4 (10, 20, and 30 μg/mL) at 37 °C for 3 h duration, separately. The cells were then washed with PBS and mixed with 0.4% trypan blue dye in equal ratios. After a brief incubation at 37 °C the live and dead cells were scored with the help of a hemocytometer. The results are presented as a percentage of dead cells.

Apoptosis Analysis by Acridine Orange/Ethidium Bromide (AO/EtBr) Staining with Fluorescence Microscopy. A 1 × 10⁶ number of viable DLA cells were incubated for 3 h with increasing concentrations of 1–4 (20, 30 μg/mL) at 37 °C separately. The cells were then washed with PBS, and 40 μL of AO/EtBr solution (1 part of 100 μg/mL of AO in PBS; 1 part of 100 μg/mL of EtBr in PBS) was added just prior to fluorescence microscopy examination. The cells were spread on a slide and examined under a fluorescence microscope. Images were captured by a Nikon 800 fluorescence microscope at 20 and 40× magnifications.

DNA Fragmentation Assay. Electrophoretic analysis of the fragmented DNA was performed for apoptotic studies. Total nuclear DNA isolated from DLA cells were estimated following the procedure described by Kuo et al.²⁶ The cells were treated with different

Scheme 1. Synthesis of Complexes of 1–4



concentrations of complexes (10, 20, and 30 $\mu\text{g/mL}$) for 3 h. After lysis of the DL cells using 1 mL of lytic buffer [20 mM Tris-Cl (pH ~ 7.5), 0.15 M NaCl, 1 mM EDTA, 1% SDS] at 4 $^\circ\text{C}$ for 30 min and centrifugation ($3,000 \times g$ for 10 min, rt), the supernatant was separated, and 20 μL proteinase K (stock 20 mg/mL) added to it followed by incubation for 3 h at 37 $^\circ\text{C}$. Again, it was centrifuged at $12,000 \times g$ for 10 min at rt and supernatant collected in another tube, DNA precipitated by addition of chilled absolute ethanol and 0.1 M NaCl. It was collected by centrifugation and washed thoroughly with 70% ethanol, and the pellet thus obtained dried and dissolved in distilled water. DNA samples were prepared in a loading solution (0.25% bromophenol blue, 0.25% xylene cyanol FF and 30% glycerol) in 1:5 ratio and 10 μL of samples loaded in each well of 1.8% agarose gel containing 0.5 $\mu\text{g/mL}$ ethidium bromide. Electrophoresis was carried out in TAE buffer for 1.5 h. The DNA bands in gel were observed and photographed in a Gel documentation system (G: BOX, SYNGENE).

RESULTS AND DISCUSSION

Synthesis and Characterization. 4-(2-Methoxyphenyl)-benzaldehyde reacted with an excess of pyrrole in presence of catalytic amounts of trifluoroacetic acid (TFA) to afford 4-(2-methoxyphenyl)dipyrrromethane in reasonably good yield.²⁷ Further, two new ligands 4-(3-methoxyphenyl)dipyrrromethane and 4-(4-methoxyphenyl)dipyrrromethane have also been prepared under analogous conditions (experimental details are given in the Supporting Information). Reactions between the chloro bridged dimeric ruthenium [$\{(\eta^6\text{-arene})\text{Ru}(\mu\text{-Cl})\text{Cl}_2\}_2$] ($\eta^6\text{-arene} = \text{C}_6\text{H}_6, \text{C}_{10}\text{H}_{14}$) and structurally analogous rhodium/iridium complexes [$\{(\eta^5\text{-C}_5\text{Me}_5)\text{M}(\mu\text{-Cl})\text{Cl}_2\}_2$] [$\text{M} = \text{Rh}, \text{Ir}$] with 2-pcdpm, obtained in situ by oxidation of 4-(2-methoxyphenyl)-phenyl-dipyrrromethane with DDQ in $\text{CH}_2\text{Cl}_2/\text{CH}_3\text{OH}$ (1:1, v/v) in presence of triethylamine at rt gave neutral heteroleptic dipyrinato complexes [$(\eta^6\text{-arene})\text{-RuCl}(2\text{-pcdpm})$] and [$(\eta^5\text{-C}_5\text{Me}_5)\text{MCl}(2\text{-pcdpm})$] ($\eta^6\text{-arene} = \text{C}_6\text{H}_6, \text{1; C}_{10}\text{H}_{14}, \text{2; M} = \text{Rh}, \text{3; Ir}, \text{4}$) in moderate to good yields (48–55%, Scheme 1). On the other hand, reactions of 4-(3-methoxyphenyl)dipyrrromethane and 4-(4-methoxyphenyl)dipyrrromethane with [$\{(\eta^6\text{-C}_{10}\text{H}_{14})\text{Ru}(\mu\text{-Cl})\text{Cl}_2\}_2$] exclusively gave the complex [$(\eta^6\text{-C}_{10}\text{H}_{14})\text{RuCl}(4\text{-OH-pdpm})$] (5) in poor yield (Supporting Information, page no. 2). Both the ligands afforded same complex 5 because of cleavage of etheratic C–O–C bond (Supporting Information, Scheme S1 and S2). The complexes 1–4 are air-stable, nonhygroscopic, orange red crystalline solids, soluble in common organic solvents like methanol, ethanol, acetone,

dichloromethane, chloroform, dimethyl formamide, dimethylsulfoxide, and insoluble in diethyl ether, petroleum ether, and hexane.

Characterization of the ligands and complexes have been achieved by satisfactory elemental analyses, spectral [ESI-MS, IR, ^1H , ^{13}C , $^1\text{H}\text{-}^1\text{H}$ (COSY) NMR, UV/vis] and electrochemical (cyclic voltammetry (CV) and differential pulse voltammetry (DPV)) studies. Further, structures of 3 and 4 have been authenticated by X-ray single crystal analyses. The FT-IR spectra exhibited characteristic bands assignable to $\nu(\text{C}=\text{N}_{\text{pyrrolic}})$ pyrrolic ring vibrations at (1547, 1; 1546, 2; 1541, 3; 1542, 4 cm^{-1}) along with bands due to other moieties and suggested coordination of 2-pcdpm with respective metal centers.^{13,15}

NMR Spectral Studies. Information about composition and identities of the ligand and complexes has been obtained from ^1H , ^{13}C and $^1\text{H}\text{-}^1\text{H}$ (COSY) NMR spectral studies. Resulting data is summarized in experimental section and spectra given in the Supporting Information (Figure S9–S21). The protons due to 2-pcdpm resonated toward downfield side relative to uncoordinated ligand and appeared at $\delta \sim 5.30, 6.50, 6.67, 7.05, 7.37, 7.61, 7.79, 8.03,$ and 8.66 ppm in complexes 1 and 2.^{13,15} It may be ascribed to the coordination of 2-pcdpm to metal center ruthenium. On the other hand, arene protons displayed an upfield shift relative to respective precursor complexes [5.37 ppm, $\text{C}_6\text{H}_6, \text{1; 1.10, CH}(\text{CH}_3)_2; 2.26$ ppm $\text{C}-\text{CH}_3; 2.40, \text{CH}(\text{CH}_3)_2; 5.32$ ppm (merged with a signal due to $-\text{OCH}_2$) $\text{C}_6\text{H}_4, \text{2}$].¹⁵ In the ^1H NMR spectra of 3 and 4, protons due to 2-pcdpm exhibited a little upfield shift [5.28, 6.44, 6.57, 7.04, 7.34, 7.57, 7.76, and 8.62 ppm] relative to the free ligand and 1 or 2. In a similar manner, the protons due to Cp^* in 3 and 4 displayed an upfield shift of ~ 0.09 ppm and resonated at almost the same position [$\delta \sim 1.48$ ppm] with respect to the metal precursor complexes, indicating a rather small change in the electronic environment about the metal centers. A shift in the position of 4-(2-methoxyphenyl)dipyrrromethane and η^n -bonded hydrocarbons may be ascribed to complexation of the ligand with the metal center and formation of respective complexes. Further, to affirm the merger of one of the pyridyl protons in 3 and 4, we have recorded ^1H NMR of 4 in $\text{DMSO-}d_6$ (Supporting Information, Figure S20). ^{13}C NMR and 2D ($^1\text{H}\text{-}^1\text{H}$) spectral data of 1–4 further supported the formation of complexes and the proposed formulations.^{13,15}

Crystal Structures. The structures of 3 and 4 have been determined crystallographically. Details about data collection,

solution and refinement are summarized in Table 1. Selected geometrical parameters are given in Table 2, and pertinent

Table 1. Crystal Data and Structure Refinement Parameters for 3 and 4

	C ₃₁ H ₃₁ ClRhN ₃ O	C ₃₁ H ₃₁ ClIrN ₃ O
empirical formula	C ₃₁ H ₃₁ ClRhN ₃ O	C ₃₁ H ₃₁ ClIrN ₃ O
crystal system	monoclinic	monoclinic
space group	P2 ₁ /c	P2 ₁ /c
a (Å)	10.560(2)	10.536(2)
b (Å)	18.195(4)	18.093(4)
c (Å)	14.774(3)	14.968(3)
α (deg)	90.00	90.00
β (deg)	92.10(3)	92.20(3)
γ (deg)	90.00	90.00
V (Å ³), Z	2836.9(10), 4	2851.2(10), 4
λ (Å)	0.71073	0.71073
color and habit	red, block	red, block
T (K)	153(2)	153(2)
reflins collected	6504	6525
reflins/restraint/params	5965/0/339	6506/0/339
D _{calcd} (Mg m ⁻³)	1.405	1.606
μ (mm ⁻¹)	0.724	4.804
GOF on F ²	1.028	1.053
final R indices I > 2σ(I)	R1 = 0.0382 wR2 = 0.0835	R1 = 0.0329 wR2 = 0.0751
R indices (all data)	R1 = 0.0502 wR2 = 0.0932	R1 = 0.0415 wR2 = 0.0804

Table 2. Selected Bond Lengths (Å) and Angles (deg) for 3 and 4^a

	3		4	
	Bond Length (Å)			
Rh–N1	2.09(5)	Ir–N1	2.08(3)	
Rh–N2	2.08(5)	Ir–N2	2.08(3)	
Rh–Cl1	2.40(15)	Ir–Cl1	2.40(11)	
C23–O1	1.37(6)	C23–O1	1.36(5)	
C27–N3	1.32(9)	C27–N3	1.33(6)	
C31–N3	1.33(9)	C31–N3	1.34(6)	
Rh–C _g	1.79	Ir–C _g	1.79	
Rh–C _{av}	2.16	Ir–C _{av}	2.16	
	Bond Angle (deg)			
N2–Rh1–N1	92.58(15)	N2–Ir1–N1	84.24(13)	
N2–Rh1–Cl1	91.53(12)	N2–Ir1–Cl1	88.95(9)	
N1–Rh1–Cl1	90.32(14)	N1–Ir1–Cl1	87.65(10)	
C23–O1–C26	117.4(4)	C23–O1–C26	117.6(3)	
C27–N3–C31	117.01	C27–N3–C31	116.14	
C11–N1–C14	107.72	C11–N1–C14	106.81	
ω	69.70	ω	70.97	

^aC_g = metal centroid bond distance, C_{av} = average metal–carbon bond distance, ω = the twist angle between dipyrin core and *meso*-phenyl substituent.

views depicted in Figure 1. Both the complexes 3 and 4 crystallize in the monoclinic system with P2₁/c space group. Crystal structures revealed typical “piano-stool” geometry about the metal center in both 3 and 4. The coordination site about the metal center in these complexes are occupied by two pyrrolic nitrogens from 2-pcdpm, a chloro group and pentamethylcyclopentadienyl (Cp*) ring in η⁵-manner. The Rh–N and Rh–Cl bond distances in 3 [Rh–N1, 2.09 Å; Rh–N2, 2.08 Å; Rh–Cl1, 2.40 Å] are normal and consistent with

other related systems.^{15,28} The N–Rh–N and N–Rh–Cl angles are close to 90° [N1–Rh–N2, 92.58°; N1–Rh–Cl1, 91.53°; N2–Rh–Cl1, 90.32°] and suggested a “piano stool” geometry about the metal center (Table 2) with average Rh–C bond distances of 2.16 Å [range, 2.155–2.178 Å]. The Cp* ring is almost planar, and the rhodium center in 3 is displaced from centroid of the Cp* ring by 1.79 Å, which is normal and comparable to values reported in other rhodium complexes.^{15,28}

The *meso*-phenyl substituent in 3 is twisted out of plane by 69.70° with respect to the dipyrin moiety. These are close to the values reported in other (η⁵-C₅H₅)Rh(III)- complexes.^{15,28}

Likewise, Ir–N and Ir–Cl bond distances in 4 [Ir–N1, 2.08 Å; Ir–N2, 2.08 Å; Ir–Cl1, 2.40 Å] are normal and comparable to other related systems.^{15,28} The centroid of the Cp* ring is separated from the metal center by 1.79 Å. The N–Ir–N and N–Ir–Cl bond angles in 4 are less than 90° [N1–Ir–N2, 84.24°; N1–Ir–Cl1, 87.65°; N2–Ir–Cl1, 88.95°] and consistent with a “piano stool” arrangement of the various groups about the metal center. The *meso*-phenyl substituent is twisted out of plane with respect to dipyrin unit by 70.97°. Average Ir–C bond distances in 4 are 2.16 Å [range 2.155–2.219 Å].^{15,28}

The crystal structures of 3 and 4 revealed the presence of extensive intermolecular C–H⋯Cl interactions leading to the formation of the head to tail structural motif shown in Figure 2. The C–H⋯Cl interaction distances are less than the sum of van der Waals radii [3.572, 3; 3.581 Å, 4] and lie within the reported range.²⁹

■ ELECTRONIC ABSORPTION SPECTROSCOPY

The electronic absorption spectra of 1–4 were acquired in (EtOH:H₂O, *c*, 10 μM; 1:1, *v/v*; pH ~ 7.3), and the resulting spectra is depicted in Figure 3. The intense low energy bands displayed by complexes [487, 432, 1; 489, 431, 2; 488, 436, 3; 496, 413 nm 4] may be assigned to conjugated dipyrin based π–π* and metal to ligand charge transfer (MLCT) transitions in the visible region, while high energy bands [358, 260, 1; 351, 260, 2; 353, 259, 3; 357, 260 nm 4] to dipyrin based intraligand π–π* transitions.^{13,15,28}

UV/vis Titration Studies. Electronic absorption spectroscopy is one of the most widely used techniques to follow the interaction of metal complexes with DNA. The binding of metal complexes with DNA usually takes place through both covalent and/or noncovalent interactions.³⁰ In covalent interactions the labile group of complexes is replaced by a nitrogen donor atom from the nucleotide, while noncovalent interactions occur via intercalative, electrostatic, and groove binding. It has been observed that strong stacking interaction between the complexes and DNA base pairs/contraction of DNA helix/conformational changes lead to hypochromism. On the other hand hyperchromism in absorption bands indicate minor groove binding, unwinding of DNA double helix, simultaneous exposure of the DNA bases, and damage to the DNA double helix.³¹ Therefore, absorption titration studies have been made to investigate the binding mode, intrinsic equilibrium binding constant (K_b), and binding site size (*s*) for the complexes with CT DNA.³²

The absorption spectra of 1–4 (*c*, 10 μM) in the presence of varying concentration of CT DNA (*c*, 1–10 μM) is shown in Figure 4, and the resulting data summarized in Table 3. In its absorption spectra 1 exhibited four bands at 260, 358, 432, and 487 nm. Upon addition of CT DNA (1 μM) the intraligand band (260 nm) of 1 exhibited hyperchromism (*ε*, 0.1165–

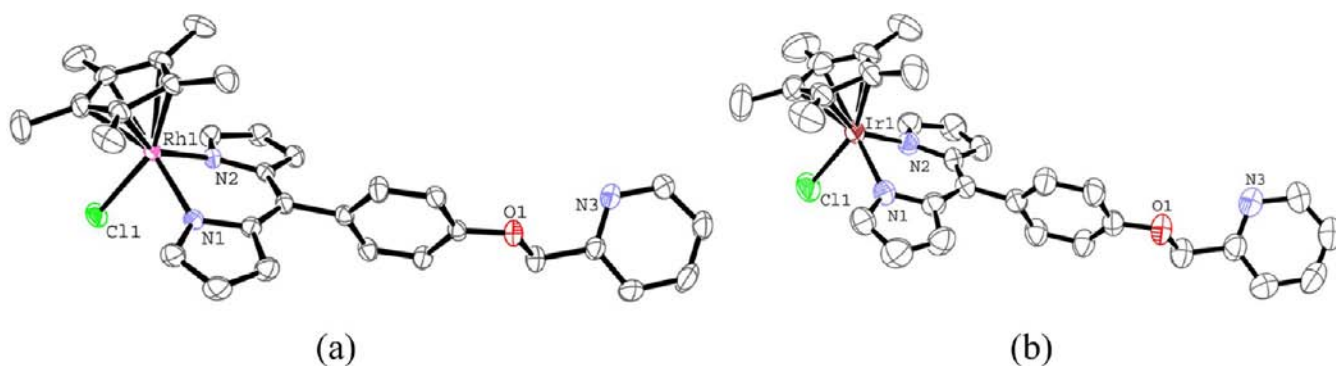


Figure 1. ORTEP diagrams of 3 (a) and 4 (b) at 30% thermal ellipsoid probability (H-atoms omitted for clarity).

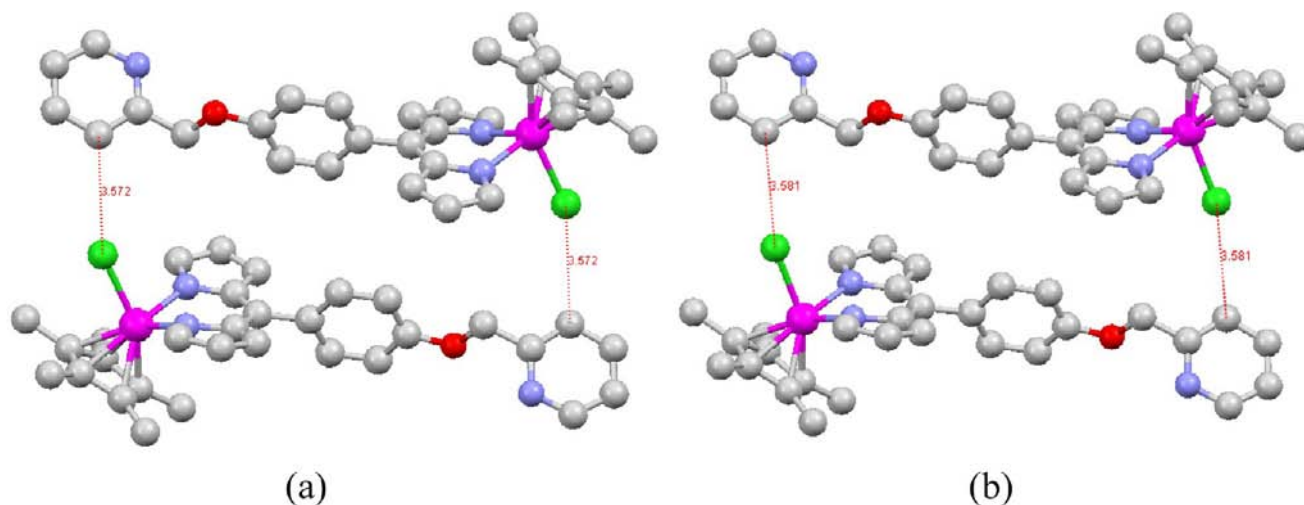


Figure 2. Head to tail arrangement in 3 (a) and 4 (b) resulting from C–H...Cl interactions.

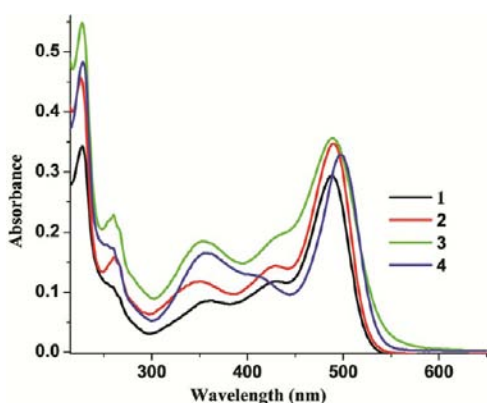


Figure 3. Electronic spectra of 1–4 in ((EtOH:H₂O, *c*, 10 μM; 1:1, *v/v*; pH ~ 7.3).

0.1409) with a blue shift of ~1 nm (~259 nm). Further, additions of CT DNA (2–10 μM) lead to a hyperchromic shift of the band at 260 nm along with a blue shift of ~4 nm to appear at ~256 nm (ϵ , 0.7392). However, the bands at 358, 432, and 487 nm do not show any appreciable change. Similarly addition of CT DNA (1 μM) to a solution of 2 leads to hyperchromic shift in the position of the transitions at 260 and 351 nm along with a blue shift of ~3 nm and ~17 nm [~257 (ϵ , 0.1732–0.4188), ~334 nm (ϵ , 0.1279–0.1902)]. Further addition of DNA (2–10 μM) leads to a hyperchromic shift for the bands at 260 and 351 nm along with a blue shift of ~5 and

~24 nm [~255 (ϵ , 2.4500), ~327 nm (ϵ , 0.7909)], while the bands at 431 and 489 nm do not show any significant shift. Notably, 3 and 4 exhibited quite different behavior in CT DNA titration studies. Addition of CT DNA (1 μM) to a solution of 3 leads to a hyperchromic shift of the band at 259 nm (ϵ , 0.11762–0.2374). Further increase in the concentration of CT DNA (2–10 μM) causes a concomitant increase in the absorbance intensity for the band at 259 nm (ϵ , 0.7082) without any significant shift. Complex 4 exhibited similar behavior under analogous conditions. The observed hyperchromism in 1 and 2 with a blue shift suggested that these bind to CT DNA by external contact, possibly electrostatic binding. Overall, results suggested that although 1–4 interact considerably with CT DNA, the extent of interaction is different for 3 and 4 (may be weaker) relative to 1 and 2.

Intrinsic equilibrium binding constant (K_b) and binding site size (*s*) have also been derived (5.6×10^{-5} , 0.15, 1; 2.8×10^{-6} , 0.14, 2; 3.2×10^{-4} , 0.12, 3; 4.5×10^{-4} , 0.13, 4) and these are consistent with other reports.³³ High binding constant (K_b) for 2 indicated its greater affinity for DNA that may be attributed to steric hindrance imposed by coordinated arene. Lower value of *s* also indicated groove binding and/or surface binding of the complexes to DNA. The intrinsic binding constants suggested that binding affinity of complexes lies in the order of 2 > 1 > 4 > 3.

Electrochemical Studies. The redox behavior of 1–4 has been studied by CV and DPV in MeCN at rt, and the resulting data is gathered in Supporting Information, Table S5. These

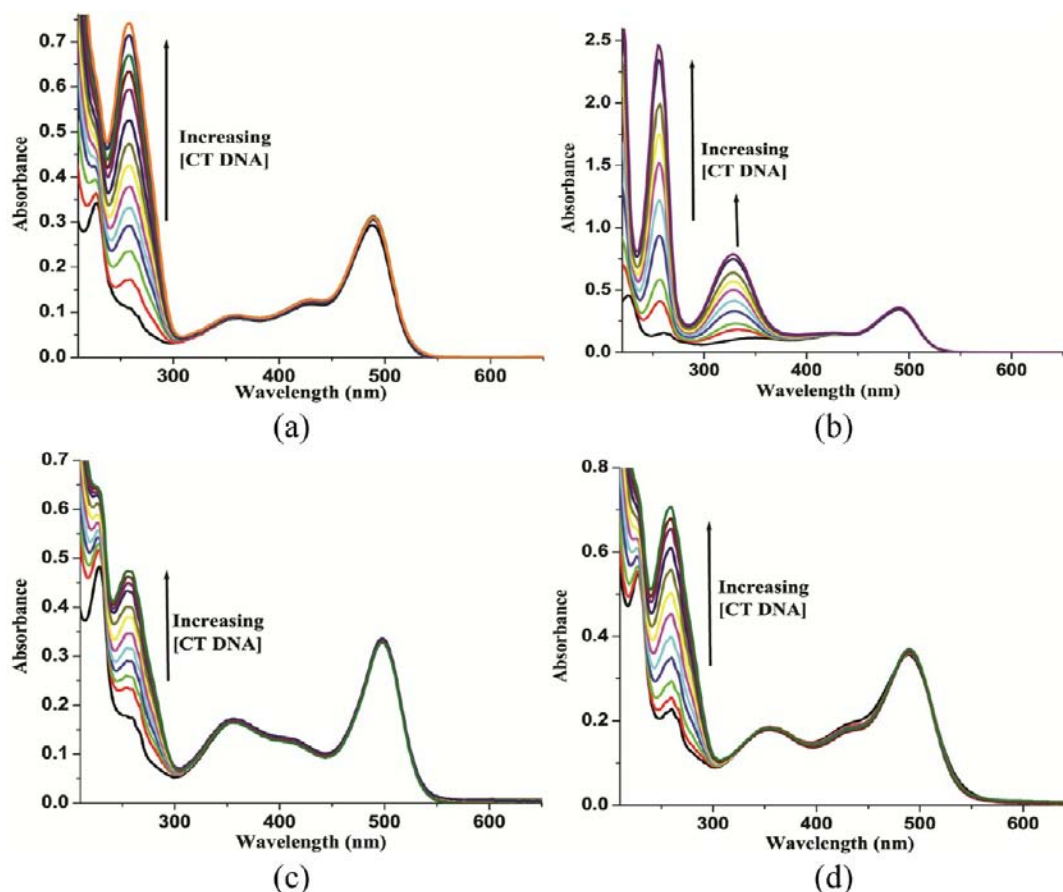


Figure 4. Absorption titration spectra of **1** (a), **2** (b), **3** (c), and **4** (d) in EtOH:H₂O (1:1) with an increase in molar concentration ratio of CT DNA to complex (1–10 μ M) at rt. Arrow shows absorbance changes upon increasing CT DNA concentration.

Table 3. Absorption Spectral Properties of **1–4** Bound to CT DNA

complexes	λ_{\max} (nm)	changes in absorbance	$\Delta\epsilon$ M ⁻¹ cm ⁻¹	blue shift (nm)	K_b (M ⁻¹)	site size (<i>s</i>)
1	260	hyperchromism	0.6176	4	5.6×10^{-5}	0.15
2	260	hyperchromism	2.2768	5	2.8×10^{-6}	0.14
3	259	hyperchromism	0.3040	no shift	3.2×10^{-4}	0.12
4	260	hyperchromism	0.5715	no shift	4.5×10^{-4}	0.13

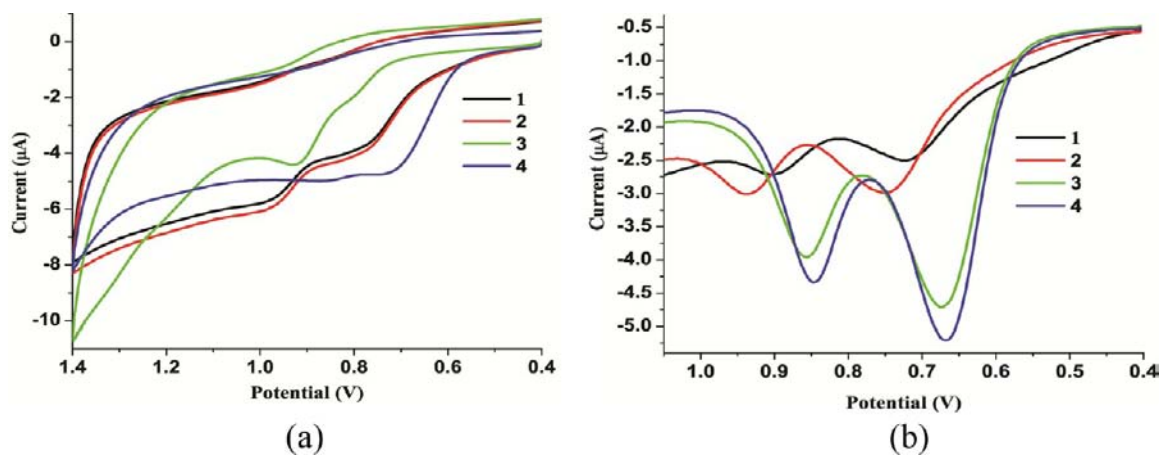


Figure 5. Cyclic (a) and differential pulse voltammograms (b) of **1–4** in MeCN (*c*, 100 μ M).

exhibited two irreversible oxidation waves in the range 0.0–1.4 V vs Ag/Ag⁺.^{15,34} The first irreversible oxidation wave ($E_{pa} = 0.744$, **1**; 0.760, **2**; 0.803, **3**; and 0.662 V, **4**) has been assigned

to dpm/dpm⁺, while the second one ($E_{pa} = 0.985$, **1**; 0.982, **2**; 0.916, **3**; 0.838 V, **4**) to metal based oxidations [Ru²⁺/Ru³⁺, **1** and **2**; Rh³⁺/Rh⁴⁺, **3**; Ir³⁺/Ir⁴⁺, **4**]. Accordingly in their DPV

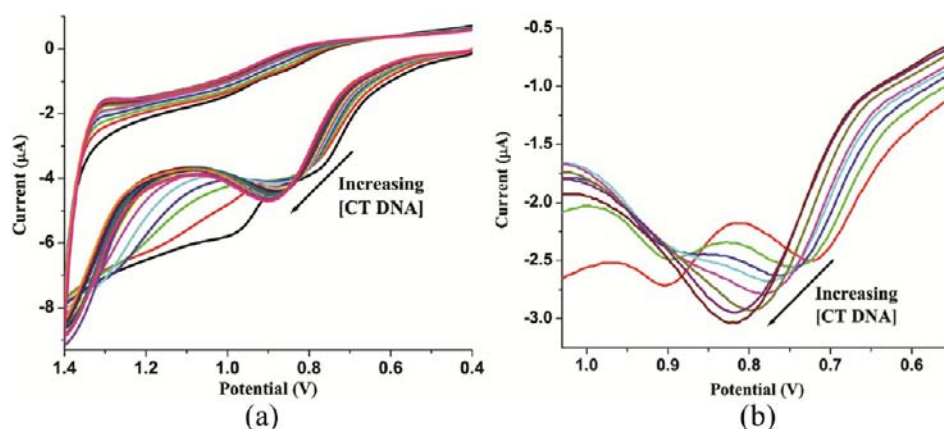


Figure 6. Evolution of the CV (a) and DPV (b) of **1** (*c*, 100 μM , MeCN) in the presence of CT DNA (0.0–1.0 μM), at rt.

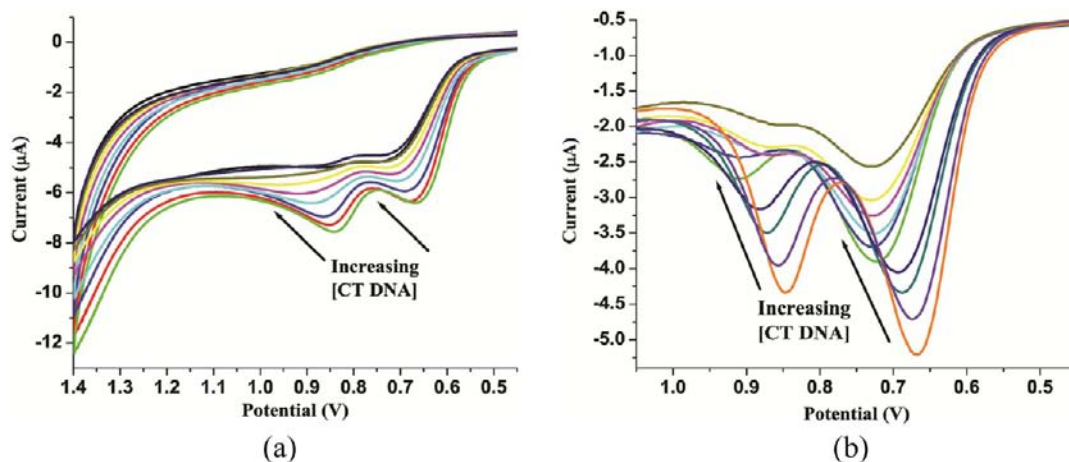


Figure 7. Evolution of the CV (a) and DPV (b) of **4** (*c*, 100 μM , MeCN) in presence of CT DNA (0.0–1.0 μM), at rt.

1–4 exhibited oxidation peaks associated with dpm/dpm^+ (E_{pa} , 0.717, **1**; 0.749, **2**; 0.672 **3**; 0.666 V, **4**), $\text{M}^{2+}/\text{3}^{+}$ (0.903, **1**; 0.936, **2**), and $\text{M}^{3+}/\text{4}^{+}$ (0.857, **3**; 0.855 V, **4**) redox couples (Figure 5). However, **1–4** do not show any significant redox wave in a negative potential window.

Since **1–4** possesses redox active moieties, therefore their electrochemical properties are expected to be altered in the presence of DNA as can be followed by CV and DPV studies. The oxidative wave due to dpm/dpm^+ couple (E_{pa} , 0.744 V) in the cyclic voltammogram of **1** showed a positive potential shift with an increase in current intensity (E_{pa} , 0.782 V; ΔE_{pa} , 0.038 V, ΔI , 9%) upon addition of 0.1 μM CT DNA. On the other hand, the wave due to metal based oxidation ($\text{Ru}^{2+}/\text{Ru}^{3+}$) exhibited a negative potential shift with decrease in current intensity (E_{pa} , 0.985 to 0.976 V; ΔE_{pa} , 0.011 V, ΔI 13%). Further additions of CT DNA (0.2–1.0 μM) led to the disappearance of both the oxidative waves associated with **1** (dpm/dpm^+ and $\text{Ru}^{2+}/\text{Ru}^{3+}$ redox couple) and the emergence of a new intense oxidative wave at E_{pa} , 0.891 V (ΔE_{pa} , 0.147 V, ΔI 23%). The significant changes in both the redox couples strongly suggested some sort of interactions between **1** and CT DNA. Accordingly in DPV, the peak due to dpm/dpm^+ displayed a positive potential shift with an increase in current intensity (E_{pa} , 0.729 V; ΔE_{pa} , 0.012 V, ΔI , 12%), and a peak due to $\text{Ru}^{2+}/\text{Ru}^{3+}$ (E_{pa} , 0.899 V) showed a negative potential shift (E_{pa} , 0.891 V; ΔE_{pa} , 0.008 V, ΔI , 11%) upon addition of CT DNA (0.1 μM). Further, increasing the concentration of

CT DNA (0.2–1.0 μM) leads to the appearance of a new oxidative peak at E_{pa} 0.819 V (ΔE_{pa} , 0.174 V, ΔI , 26%), and both peaks due to **1** disappeared (Figure 6). Similar trends have been observed for **2** upon addition of CT DNA under analogous conditions (Supporting Information, Figure S22).

Upon addition of CT DNA (0.1 μM) to a solution of **3** the oxidation wave due to $\text{Rh}^{3+}/\text{Rh}^{4+}$ redox couple (E_{pa} , 0.916 V) exhibited a positive potential shift and a decrease in the current intensity (E_{pa} 0.926, ΔE_{pa} , 0.010 V, ΔI , 8%). Further additions of CT DNA (0.2–1.0 μM) causes gradual decrease in the current intensity as well as a more positive potential shift in the oxidative wave to appear at E_{pa} 0.980 V (ΔE_{pa} , 0.064 V, ΔI 59%). In sharp contrast, addition of CT DNA (0.1 μM) to **4** leads to a positive potential shift along with a decrease in current intensity for dpm/dpm^+ (E_{pa} , 0.662 V; ΔE_{pa} , 0.011 V, ΔI 7%) and $\text{Ir}^{3+}/\text{Ir}^{4+}$ (E_{pa} , 0.838 V; ΔE_{pa} , 0.08 V, ΔI 9%) redox couples. Further, addition of CT DNA (0.2–1.0 μM) displayed successive positive potential shift with decrease in the current intensity to appear at E_{pa} 0.751 V (ΔE_{pa} , 0.089 V, ΔI 69%) and (E_{pa} 0.935 V; ΔE_{pa} , 0.092 V, ΔI 64%).

Similarly, in DPV of **3** both the oxidation peak assignable to dpm/dpm^+ and $\text{Rh}^{3+}/\text{Rh}^{4+}$ at E_{pa} , 0.672 and 0.855 V, showed positive potential shift with simultaneous decrease in current intensity upon addition of 0.1 μM CT DNA (E_{pa} 0.679 V; ΔE_{pa} , 0.007 V, ΔI 9%, dpm/dpm^+ ; and E_{pa} 0.861, ΔE_{pa} , 0.006 V, ΔI 9%, $\text{Rh}^{3+}/\text{Rh}^{4+}$). Further, addition of CT DNA (0.2–1.0 μM) displayed successive positive potential shift and decrease in

current intensity (E_{pa} 0.724, ΔE_{pa} 0.052 V, ΔI 47%, dpm/dpm⁺; 0.876, ΔE_{pa} 0.021 V, ΔI 41%; Rh³⁺/Rh⁴⁺, Supporting Information, Figure S23). Similar trends were observed for 4 under analogous conditions (Figure 7). It is worth mentioning that electrochemical studies also indicated that the extent of interaction of 1 and 2 is greater with CT DNA relative to 3 and 4, which may be attributed to the oxidation state of the respective metal ions. The electrochemical studies corroborated well with the electronic absorption studies and thereby authenticate the strong interaction of CT DNA with complexes 1–4. The cytotoxicity of complexes increases with increase in reduction potential or easily oxidizable species.³⁵ It is possible to correlate the redox potential with cytotoxicity. From CV data it is clear that the oxidizing tendency of 1–4 lies in the order 4 > 2 > 1 > 3 (0.744, 1; 0.760, 2; 0.803, 3; 0.662 V, 4) based on the dpm moiety. Therefore, on the basis of the electrochemical data the complexes 1–4 demonstrate the cytotoxicity order 4 > 2 > 1 > 3.

Mass Spectral Studies. The ESI-MS of 1–4 have been acquired to understand the relative composition and stability of the complexes. Notably these displayed the most abundant peaks at m/z 506.0030 (1, M–Cl⁺), 562.1433 (2, M–Cl⁺), 564.1526 (3, M–Cl⁺), and 654.2090 (4, M–Cl⁺) suggesting cleavage of the M–Cl bond and loss of chloro group from respective complexes. However, we do not get the molecular ion peak in these complexes (Supporting Information, Figure S24–S27). The results strongly suggest that the chloro group in these complexes is highly labile.

Partition Coefficient Determination. Lipophilicity is the fundamental physicochemical property and illustrates the ability of a drug to cross lipid bilayers and determines the fate of a drug in the body by several ADME aspects like the absorption, distribution metabolism, and excretion processes.³⁶ The *n*-octanol/water partition coefficient (*P*) parameters are generally used for the measurement of lipophilicity.²⁴ Partition coefficients, *P*, were measured to conclude the permeation behavior of 1–4 through a biological membrane.³⁷ The *P* measurements are based on solubility of a given compound in an aqueous vs organic medium.³⁸ The determined log *P* values are given in Table 4, and these lie in the range of reported

Table 4. Log *P* Values for Complexes 1–4^a

complex	log <i>P</i>	
	mean	SD
1	1.27	0.03
2	1.28	0.02
3	1.26	0.01
4	1.27	0.03

^aResults are the mean values obtained from three independent experiments and are expressed as mean ± SD.

values.³⁹ These results are also consistent with trypan blue exclusion assay (cytotoxicity) of the complexes increases with increases in lipophilicity. Since 1–4 exhibit poor solubility (almost insoluble) in water, we could not look into their aqueous solution chemistry (with respect to hydrolysis and arene loss).⁴⁰

Cytotoxicity of Compounds on DLA Cells in vitro. A trypan blue exclusion assay was performed to measure the cytotoxicity and DLA cell viability in response to treatment with the compounds under investigation at 10, 20, and 30 μg/mL concentrations and the ensuing data is depicted in Figure 8.

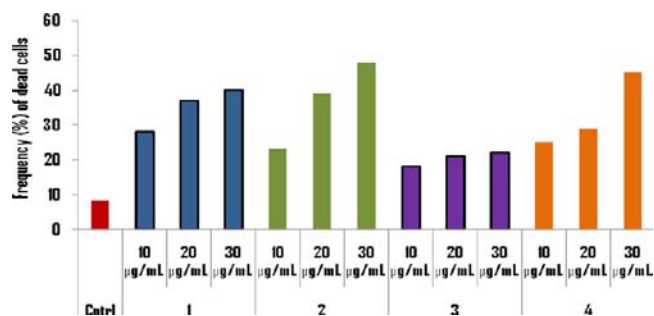


Figure 8. Trypan blue exclusion assay was performed to measure cell viability in DLA cells in response to compounds 1–4 with 3 h of incubation.

The frequency of dead cells increases with an increase in concentration of the compounds. Maximum frequency of dead cells is shown by 2 followed by 4, compound 1 showed potential toxicity at higher concentrations, but 3 appears to be less active; enhancement of toxicity (cell death) is dose dependent.

Cell Morphology Analysis. Apoptosis is a dependable marker for the evaluation of potential of anticancer drugs.⁴¹ Morphological changes of the apoptosis can be visualized in either fixed tissue or live cells grown in a culture by examining nuclear morphology using vital dyes.⁴² Phase contrast and fluorescence microscopy are widely used for investigating intracellular morphological changes.⁴³ Cell morphology analysis by fluorescence (AO/EtBr) staining (Figure 9) showed noticeable morphological changes in the nucleus, internal organelle, and plasma membrane integrity caused by 1–4 in live DL cells. The untreated DL cells showed uniform green fluorescence, indicating evenly distributed chromatin in the nucleus of healthy cells. After treatment with 1–4 at different concentrations, DLA cells displayed congregated chromatin and nucleus pyknosis, a phenomenon of early apoptosis as showed by the emitted bright fluorescence. Marked nuclear condensation, membrane blebbing, nuclear fragmentation, and apoptotic bodies became prominent in compound 2 and 4 treated cells and turned green into orangeish yellow fluorescence indicating apoptotic programmed cell death. The present study clearly demonstrated the activity of complexes in promoting these marked morphological changes in the DLA cells which ultimately leads to apoptosis.

■ APOPTOSIS INDUCTION AND DNA FRAGMENTATION ASSAY

The DNA ladder technique has been used to investigate the endonuclease activity of 1–4. A typical laddering pattern observed upon treatment of DLA cells with different concentrations of the compounds is depicted in Figure 10. DNA fragmentation is one of the characteristic features observed in apoptotic cells and is generally considered as the biochemical hallmark of the apoptosis.⁴⁴ Formation of DNA ladder in gels correlates with early morphological sign of apoptosis and has been widely used as a distinctive marker of the apoptosis process. The ladder-like appearance of DNA observed in the DL cells treated with 1–4 is an indicator of the apoptosis. This pattern of DNA fragmentation occurs by activation of endogenous nucleases that cleaves DNA in the linker region between histones on the chromosomes. Since DNA wrapped around histones comprises about 180–200 bp, multiples of these intervals are characteristically observed and

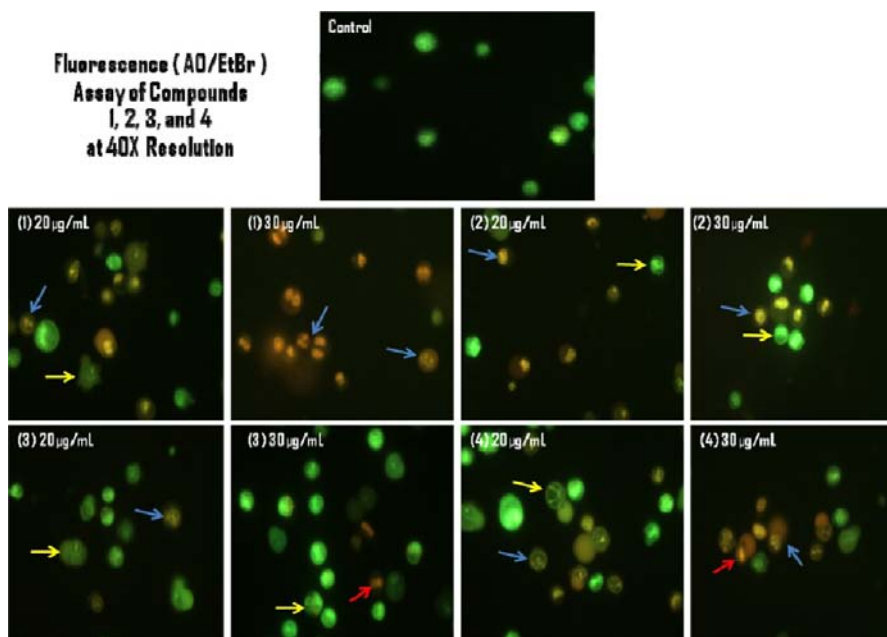


Figure 9. Fluorescent (Acridine orange/Ethidium bromide) images of control and treated DLA cells with compounds 1–4 at concentrations 20 and 30 $\mu\text{g}/\text{mL}$ after 3 h of incubation. The yellow arrows show early apoptotic cells with chromatin superaggregation, that is, highly condensed chromatin, blue arrows show late apoptotic cells with condensation and chromatin clumping, and red arrows show necrotic cells.

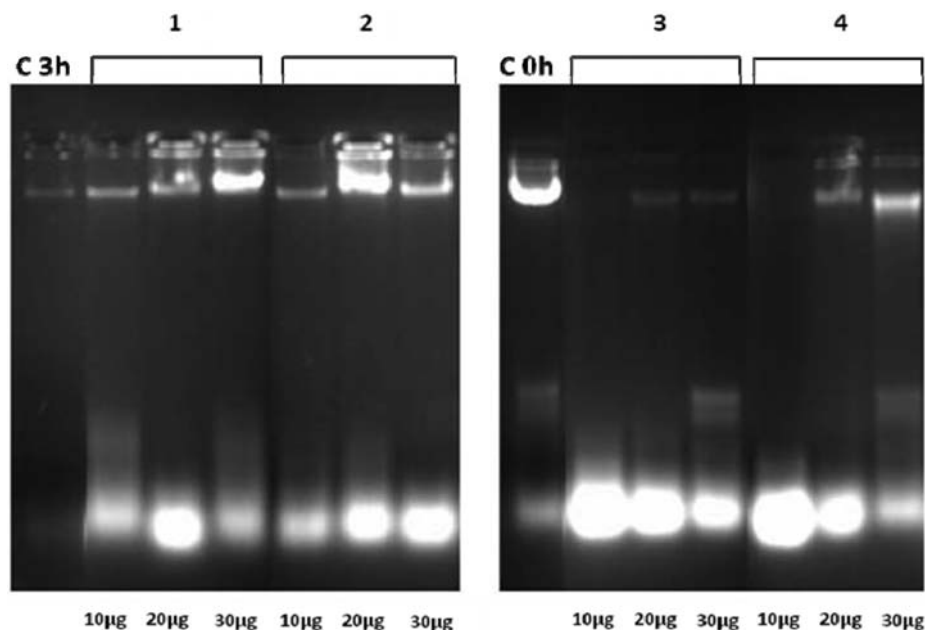


Figure 10. DNA fragmentation assay for analysis of apoptosis in DLA cells. DLA cells were treated with compounds for 3 h, and DNA was isolated. DNA from a different sample was loaded in each lane and subjected to 1.8% agarose gel electrophoresis.

are commonly referred to as “apoptotic” ladder. Once this pattern of DNA degradation begins the cells eventually die and cannot be rescued even by removal of the apoptotic signal.⁴⁵ Other reports on internucleosomal DNA cleavage during apoptosis in a wide variety of cells and tissues are numerous.⁴⁶ In contrast, DNA laddering is not seen in cells which have undergone necrosis and show a random fragmentation and histone degradation pattern leading to diffuse smears on DNA agarose electrophoresis. The necrotic DNA fragments are also larger and therefore significantly less in number, than apoptotic DNA.⁴⁷

CONCLUSIONS

In summary, four new heteroleptic “piano stool” complexes containing $(\eta^6\text{-arene})\text{Ru-}$, $(\eta^5\text{-C}_5\text{Me}_5)\text{Rh-}$, and $(\eta^5\text{-C}_5\text{Me}_5)\text{Ir-}$ moieties and 4-(2-methoxypyridyl)phenyldipyrromethene ligand have been synthesized and fully characterized. Electronic absorption and electrochemical titration studies revealed that the complexes significantly bind to DNA. From the binding constant values, it is clear that these exhibit better activity even at very low concentrations. The complexes 1–4 are highly soluble in methanol and ethanol and exhibit potential in vitro cytotoxicity and antitumor activity. The activity of these

complexes can be arranged as $2 > 1 > 4 > 3$ based on binding constant and antitumor activity. We believe that our results and elaborations may provide useful information for the design of new complexes containing dipyrins and Ru(II), Rh(III), and Ir(III) arene moieties as anticancer agents.

■ ASSOCIATED CONTENT

■ Supporting Information

CCDC deposition No. 879367 (3) and 879368 (4) contain the supplementary crystallographic data for this paper. In addition, Tables S5 and Figures S1–S27 contain the absorption plot, calibration curve, ^1H , ^1H - ^1H COSY, and ^{13}C NMR, UV/vis titration curves; CV, DPV, and HRMS are provided. This material is available free of charge via the Internet at <http://pubs.acs.org>.

■ AUTHOR INFORMATION

Corresponding Author

*Phone: + 91 542 6702480. Fax: + 91 542 2368174. E-mail: dspbhu@bhu.ac.in.

Notes

The authors declare no competing financial interest.

■ ACKNOWLEDGMENTS

The authors thank the Council of Scientific and Industrial Research, New Delhi, for financial assistance through the Scheme HRDG 01 (2361)/10/EMR-II) and for the award of a Junior Research Fellowship to R.K.G. (No. 09/013(0210)/2009-EMR-I). We also thank the Head, Department of Chemistry, Faculty of Science, Banaras Hindu University, Varanasi (U.P.), India, for extending laboratory facilities and the National Institute of Advanced Industrial Science and Technology (AIST), Osaka, Japan, for extending the single crystal X-ray facility.

■ REFERENCES

- (1) Cepeda, V.; Fuertes, M. A.; Castilla, J.; Alonso, C.; Quevedo, C.; Perez, J. M. *Anti-Cancer Agents Med. Chem.* **2007**, *7*, 3.
- (2) Giaccone, G.; Herbst, R. S.; Manegold, C.; Scagliotti, G.; Rosell, R.; Miller, V. J. *Clin. Oncol.* **2004**, *22*, 777.
- (3) (a) Gasser, G.; Ott, I.; Metzler-Nolte, N. *J. Med. Chem.* **2011**, *54*, 3. (b) Jakupec, M. A.; Galanski, M.; Arion, V. B.; Hartinger, C. G.; Keppler, B. K. *Dalton Trans.* **2008**, *2*, 183. (c) Dyson, P. J.; Sava, G. *Dalton Trans.* **2006**, 1929, and references therein.
- (4) (a) Clarke, M. J. *Coord. Chem. Rev.* **2003**, *236*, 209. (b) Smitha, G. S.; Therrien, B. *Dalton Trans.* **2011**, *40*, 10793.
- (5) (a) Bratsos, I.; Jedner, S.; Gianferrara, T.; Alessio, E. *Chimia* **2007**, *61*, 692. (b) Lentz, F.; Drescher, A.; Lindauer, A.; Henke, M.; Hilger, R. A.; Hartinger, C. G.; Scheulen, M. E.; Dittrich, C.; Keppler, B. K.; Jaehde, U. *Anti-Cancer Drugs* **2009**, *20*, 97. (c) Gianferrara, T.; Bratsos, I.; Alessio, E. *Dalton Trans.* **2009**, 7588.
- (6) Ginzinger, W.; Muhlgassner, G.; Arion, V. B.; Jakupec, M. A.; Roller, A.; Galanski, M.; Reithofer, M.; Berger, W.; Keppler, B. K. *J. Med. Chem.* **2012**, *55*, 3398.
- (7) (a) Morris, R. E.; Aird, R. E.; Murdoch, P. S.; Chen, H.; Cummings, J.; Hughes, N. D.; Parsons, S.; Parkin, A.; Boyd, G.; Jodrell, D. I.; Sadler, P. J. *J. Med. Chem.* **2001**, *44*, 3616. (b) Aird, R. E.; Cummings, J.; Ritchie, A. A.; Muir, M.; Morris, R. E.; Chen, H.; Sadler, P. J.; Jodrell, D. I. *Br. J. Cancer* **2002**, *86*, 1652.
- (8) Habtemariam, A.; Melchart, M.; Fernandez, R.; Parsons, S.; Oswald, I. D. H.; Parkin, A.; Fabbiani, F. P. A.; Davidson, J. E.; Dawson, A.; Aird, R. E.; Jodrell, D. I.; Sadler, P. J. *J. Med. Chem.* **2006**, *49*, 6858.
- (9) Bugarcic, T.; Habtemariam, A.; Stepankova, J.; Heringova, P.; Kasparkova, J.; Deeth, R. J.; Johnstone, R. D. L.; Prescimone, A.;

Parkin, A.; Persons, S.; Brabec, V.; Sadler, P. J. *Inorg. Chem.* **2008**, *47*, 11470.

(10) (a) Suss-Fink, G. *Dalton Trans.* **2010**, *39*, 1673. (b) Yan, Y. K.; Melchart, M.; Habtemariam, A.; Sadler, P. J. *Chem. Commun.* **2005**, 4764. (c) Noffke, A. L.; Habtemariam, A.; Pizarro, A. M.; Sadler, P. J. *Chem. Commun.* **2012**, *48*, 5219.

(11) (a) Bruijninx, P. C. A.; Sadler, P. J. *Adv. Inorg. Chem.* **2009**, *61*, 1. (b) Singh, S. K.; Joshi, S.; Singh, A. R.; Saxena, J. K.; Pandey, D. S. *Inorg. Chem.* **2007**, *46*, 10869. (c) Peacock, A. F. A.; Sadler, P. J. *Chem.—Asian J.* **2008**, *3*, 1890.

(12) (a) Wagner, R. W.; Lindsey, J. S. *J. Am. Chem. Soc.* **1994**, *116*, 9759. (b) Maeda, H.; Hasegawa, M.; Hashimoto, T.; Kakimoto, T.; Nishio, S.; Nakanishi, T. *J. Am. Chem. Soc.* **2006**, *128*, 10024.

(13) (a) Wood, T. E.; Thompson, A. *Chem. Rev.* **2007**, *107*, 1831. (b) Baudron, S. A. *CrystEngComm* **2010**, *12*, 2288. (c) Pogozhev, D.; Baudron, S. A.; Hosseini, M. W. *CrystEngComm* **2010**, *12*, 2238. (d) Hall, J. D.; McLean, T. M.; Smalley, S. J.; Waterland, M. R.; Telfer, S. G. *Dalton Trans.* **2010**, *39*, 437. (e) Halper, S. R.; Malachowski, M. R.; Delaney, H. M.; Cohen, S. M. *Inorg. Chem.* **2004**, *43*, 1242. (f) Halper, S. R.; Cohen, S. M. *Angew. Chem., Int. Ed.* **2004**, *43*, 2385. (g) Murphy, D. L.; Malachowski, M. R.; Campana, C.; Cohen, S. M. *Chem. Commun.* **2005**, 5506. (h) Kilduff, B.; Pogozhev, D.; Baudron, S. A.; Hosseini, M. W. *Inorg. Chem.* **2010**, *49*, 1123. (i) Mendoza, D. S.; Baudron, S. A.; Hosseini, M. W. *Inorg. Chem.* **2008**, *47*, 766. (j) Telfer, S. G.; Wuest, J. D. *Cryst. Growth Des.* **2009**, *9*, 1923. (k) Telfer, S. G.; Wuest, J. D. *Chem. Commun.* **2007**, 3166.

(14) (a) Dougan, S. J.; Habtemariam, A.; McHale, S. E.; Parsons, S.; Sadler, P. J. *Proc. Natl. Acad. Sci. U.S.A.* **2008**, *105*, 11628. (b) Therrien, B.; Ang, W. H.; Cherioux, F.; Vieille-Petit, L.; Jeanneret, L. J.; Suss-Fink, G.; Dyson, P. J. *J. Clust. Sci.* **2007**, *18*, 741. (c) Gras, M.; Therrien, B.; Suss-Fink, G.; Casini, A.; Edafe, F.; Dyson, P. J. *J. Organomet. Chem.* **2010**, *695*, 1119. (d) Govender, P.; Renfrew, A. K.; Clavel, C. M.; Dyson, P. J.; Therrien, B.; Smith, G. S. *Dalton Trans.* **2011**, *40*, 1158.

(15) (a) Yadav, M.; Singh, A. K.; Pandey, D. S. *Organometallics* **2009**, *28*, 4713. (b) Yadav, M.; Singh, A. K.; Maiti, B.; Pandey, D. S. *Inorg. Chem.* **2009**, *48*, 7593–9929. (c) Yadav, M.; Kumar, P.; Pandey, D. S. *Polyhedron* **2010**, *29*, 791. (d) Yadav, M.; Singh, A. K.; Pandey, D. S. *J. Organomet. Chem.* **2011**, *696*, 758.

(16) Ben-Effrain, S. *Tumor Biol.* **1999**, *20*, 1.

(17) Goldie, H.; Felix, M. D. *Cancer Res.* **1951**, *11*, 73.

(18) Perrin, D. D.; Armango, W. L. F.; Perrin, D. R. *Purification of laboratory chemicals*; Pergamon: Oxford, U.K., 1986.

(19) (a) Bennett, M. A.; Smith, A. K. *J. Chem. Soc., Dalton Trans.* **1974**, 233. (b) Bennett, M. A.; Huang, T. N.; Matheson, T. W.; Smith, A. K. *Inorg. Synth.* **1982**, *21*, 74. (c) Kang, W.; Moseley, K.; Maitlis, P. M. *J. Am. Chem. Soc.* **1969**, *91*, 5970. (d) Ball, R. G.; Graham, W. A. G.; Heinekey, D. M.; Hoyano, J. K.; McMaster, A. D.; Mattson, B. M.; Michel, S. T. *Inorg. Chem.* **1990**, *29*, 2023. (e) White, C.; Yates, A.; Maitlis, P. M. *Inorg. Synth.* **1992**, *29*, 228. (f) Nnamania, I. N.; Joshib, G. S.; Danquah, R. D.; Abdulmalik, O.; Asakurac, T.; Abraham, D. J.; Safo, M. K. *Chem Biodiversity* **2008**, *9*, 1762.

(20) Gupta, R. K.; Pandey, R.; Singh, R.; Srivastava, N.; Maiti, B.; Saha, S.; Li, P.; Xu, Q.; Pandey, D. S. *Inorg. Chem.* **2012**, *51*, 8916.

(21) Sheldrick, G. M. *Acta Crystallogr.* **2008**, *A64*, 112.

(22) (a) Spek, A. L. *PLATON, A Multipurpose Crystallographic Tools*; Utrecht University: Utrecht, The Netherlands, 2000. (b) Spek, A. L. *Acta Crystallogr. A* **1990**, *46*, C31.

(23) (a) Carter, M. T.; Rodriguez, M.; Bard, A. J. *J. Am. Chem. Soc.* **1989**, *111*, 8901. (b) Mcghee, J. D.; Hippel, P. H. V. *J. Mol. Biol.* **1974**, *86*, 469. (c) Nelson, D. L.; Cox, M. M. *Lehninger Principles of Biochemistry*, 4th ed.; W. H. Freeman and Company: New York, 2005; p 516.

(24) (a) OECD, *Guidelines for Testing of Chemicals*; OECD: Paris, France, 1995; Vol. 107. (b) Graham, L. P. *An Introduction to Medicinal Chemistry*; Oxford University Press: Oxford, U.K., 1995.

(25) Li, L.; Cao, W.; Zheng, W.; Fan, C.; Chen, T. *Dalton Trans.* **2012**, *41*, 12766.

- (26) Kuo, P. L.; Hsu, Y. L.; Chang, C. H.; Lin, C. C. *Cancer Lett.* **2005**, *223*, 293.
- (27) Littler, J.; Miller, M. A.; Hung, C. H.; Wagner, R. W.; O'Shea, D. F.; Boyle, P. D.; Lindsey, J. S. *J. Org. Chem.* **1999**, *64*, 1391.
- (28) (a) Prasad, K. T.; Therrein, B.; Rao, K. M. *J. Organomet. Chem.* **2010**, *695*, 1375. (b) Gupta, G.; Gloria, S.; Therrien, B.; Das, B.; Rao, K. M. *J. Organomet. Chem.* **2011**, *696*, 702. (c) Hall, J. D.; McLean, T. M.; Smalley, S. J.; Waterland, M. R.; Telfer, S. G. *Dalton Trans.* **2010**, *39*, 437. (d) Hanson, K.; Tamayo, A.; Diev, V. V.; Whited, M. T.; Djurovich, P. I.; Thompson, M. E. *Inorg. Chem.* **2010**, *49*, 6077. (e) Bronner, C.; Baudron, S. A.; Hosseini, M. W. *Inorg. Chem.* **2010**, *49*, 8659. (f) Bronner, C.; Veiga, M.; Guenet, A.; Cola, L. D.; Hosseini, M. W.; Strassert, C. A.; Baudron, S. A. *Chem.—Eur. J.* **2012**, *18*, 4041.
- (29) Desiraju, G. R.; Steiner, T. *The Weak Hydrogen Bond in Structural Chemistry and Biology*; Oxford University Press: Oxford, U.K., 1999.
- (30) Zhang, Q. L.; Liu, J. G.; Chao, H.; Xue, G. Q.; Ji, L. N. *J. Inorg. Biochem.* **2001**, *83*, 49.
- (31) (a) Mancin, F.; Scrimin, P.; Tecilla, P.; Tonellato, U. *Chem. Commun.* **2005**, 2540. (b) Tjioe, L.; Meininger, A.; Joshi, T.; Spiccia, L.; Graham, B. *Inorg. Chem.* **2011**, *50*, 4327.
- (32) (a) Long, E. C.; Barton, J. K. *Acc. Chem. Res.* **1990**, *23*, 271. (b) Pasternack, R. F.; Gibbs, E. J.; Villafranca, J. J. *Biochemistry* **1983**, *22*, 251.
- (33) Herebian, D.; Sheldrick, W. S. *J. Chem. Soc., Dalton Trans.* **2002**, 966.
- (34) (a) Yu, L.; Muthukumar, K.; Sazanovich, I. V.; Kirmaier, C.; Hindin, E.; Diers, J. R.; Boyle, P. D.; Bocian, D. F.; Holten, D.; Lindsey, J. S. *Inorg. Chem.* **2003**, *42*, 6629. (b) Goze, C.; Ulrich, G.; Ziessel, R. *J. Org. Chem.* **2007**, *72*, 313.
- (35) (a) Hall, M. D.; Hambley, T. W. *Coord. Chem. Rev.* **2002**, *232*, 49. (b) Milhazes, N.; Cunha-Oliveira, T.; Martins, P.; Garrido, J.; Oliveira, C.; Rego, A. C.; Borges, F. *Chem. Res. Toxicol.* **2006**, *19*, 1294.
- (36) (a) Yang, Y.; Engkvist, O.; Llinaas, A.; Chen, H. *J. Med. Chem.* **2012**, *55*, 3667. Theil, F. P.; Guentert, T. W.; Haddad, S.; Poulin, P. *Toxicol. Lett.* **2003**, *138*, 29.
- (37) (a) Pignatello, R.; Musumeci, T.; Basile, L.; Carbone, C.; Puglisi, G. *J. Pharm. Bioallied Sci.* **2011**, *3*, 4. (b) Fresta, M.; Guccione, S.; Beccari, A. R.; Furner, P. M.; Puglisi, G. *Bioorg. Med. Chem.* **2002**, *10*, 3871.
- (38) (a) Fatouros, D. G.; Karpf, D. M.; Nielsen, F. S.; Mullertz, A. *Ther. Clin. Risk Manage.* **2007**, *3*, 591. (b) Martins, S.; Sarmiento, B.; Ferreira, D. C.; Souto, E. B. *Int. J. Nanomed.* **2007**, *2*, 595.
- (39) (a) Liu, Z.; Habtemariam, A.; Pizarro, A. M.; Fletcher, S. A.; Kisova, A.; Vrana, O.; Salassa, L.; Bruijninx, P. C. A.; Clarkson, G. J.; Brabec, V.; Sadler, P. J. *J. Med. Chem.* **2011**, *54*, 3011. (b) Aguirre, J. D.; Angeles-Boza, A. M.; Chouai, A.; Pellois, J.-P.; Turro, C.; Dunbar, K. R. *J. Am. Chem. Soc.* **2009**, *131*, 11353. (c) Aguirre, J. D.; Angeles-Boza, A. M.; Chouai, A.; Turro, C.; Pellois, J. P.; Dunbar, K. R. *Dalton Trans.* **2009**, 10806. (d) Glans, L.; Ehnborn, A.; Kock, C. d.; Martínez, A.; Estrada, J.; Smith, P. J.; Haukka, M.; Sanchez-Delgado, R. A.; Nordlander, E. *Dalton Trans.* **2012**, *41*, 2764. (e) Vock, C. A.; Renfrew, A. K.; Scopelliti, R.; Jeanneret, L. J.; Dyson, P. J. *Eur. J. Inorg. Chem.* **2008**, 1661. (f) Melchart, M.; Habtemariam, A.; Parsons, S.; Sadler, P. J. *J. Inorg. Biochem.* **2007**, *101*, 1903.
- (40) (a) Dougan, S. J.; Melchart, M.; Habtemariam, A.; Parsons, S.; Sadler, P. J. *Inorg. Chem.* **2006**, *45*, 10882. (b) Yan, Y. K.; Melchart, M.; Habtemariam, A.; Sadler, P. J. *Chem. Commun.* **2005**, 4764. (c) Ginzinger, W.; Muuhlgassner, G.; Arion, V. B.; Jakupec, M. A.; Roller, A.; Galanski, M.; Reithofer, M.; Berger, W.; Keppler, B. K. *J. Med. Chem.* **2012**, *55*, 3398. (d) Kljun, J.; Bytzeck, A. K.; Kandioller, W.; Bartel, C.; Jakupec, M. A.; Hartinger, C. G.; Keppler, B. K.; Turel, I. *Organometallics* **2011**, *30*, 2506. (e) Liu, Z.; Habtemariam, A.; Pizarro, A. M.; Fletcher, S. A.; Kisova, A.; Vrana, O.; Salassa, L.; Bruijninx, P. C. A.; Clarkson, G. J.; Brabec, V.; Sadler, P. J. *J. Med. Chem.* **2011**, *54*, 3011. (f) Lara, S. B.; Habtemariam, A.; Clarkson, G. J.; Sadler, P. J. *Eur. J. Inorg. Chem.* **2011**, 3257. (g) Hanif, M.; Nazarov, A. A.; Hartinger, C. G.; Kandioller, W.; Jakupec, M. A.; Arion, V. B.; Dyson, P. J.; Kepplera, B. K. *Dalton Trans.* **2010**, *39*, 7345.
- (41) Taraphdar, A. K.; Roy, M.; Bhattacharya, R. K. *Curr. Sci.* **2001**, *80*, 10.
- (42) Kiechle, F. L.; Zhang, X. *Clin. Chim. Acta* **2002**, *326*, 27.
- (43) Ormerod, M. G. *J. Immunol. Methods* **2002**, *265*, 73.
- (44) Zhang, J.; Xu, M. *Cell Biol.* **2002**, *12*, 84.
- (45) Bortner, C. D.; Nicklas, B.; Oldenburg, E.; Cidlowski, J. A. *Cell Biol.* **1995**, *5*, 21.
- (46) (a) Son, Y. O.; Kim, J.; Lim, J. C.; Chung, G. H.; Lee, J. C. *Food Chem. Toxicol.* **2003**, *41*, 1421. (b) Yang, H. L.; Chen, C. S.; Chang, W. H.; Lu, F. J.; Lai, Y. C.; Chen, C. C. *Cancer Lett.* **2006**, *231*, 215. (c) Kim, J. Y.; Park, K. W.; Moon, K. D.; Lee, M. K.; Choi, J.; Yee, S. T. *Food Chem. Toxicol.* **2008**, *46*, 3753. (d) Liu, C. H.; Huang, L. J.; Kuo, S. C.; Lee, T. H.; Tsai, K. J.; Chan, H. C. *Bioorg. Med. Chem.* **2009**, *17*, 42.
- (47) Allen, R. T.; Hunter, W. J., III; Agarwal, D. K. *J. Pharmacol. Toxicol. Methods* **1997**, *37*, 215.